



Nonplanar flow-induced vibrations of a cantilevered PIP structure system concurrently subjected to internal and cross flows

Z. Y. Liu^{1,2} · T. L. Jiang^{1,2} · L. Wang^{1,2} · H. L. Dai^{1,2}

Received: 28 December 2018 / Revised: 10 April 2019 / Accepted: 15 April 2019 / Published online: 24 June 2019
© The Chinese Society of Theoretical and Applied Mechanics and Springer-Verlag GmbH Germany, part of Springer Nature 2019

Abstract

Pipe-in-pipe (PIP) structures are widely used in offshore oil and gas pipelines to settle thermal insulation issues. A PIP structure system usually consists of two concentric pipes and one softer layer for thermal insulation consideration. The total response of the system is related to the dynamics of both pipes and the interactions between these two concentric pipes. In the current work, a theoretical model for flow-induced vibrations of a PIP structure system is proposed and analyzed in the presence of an internal axial flow and an external cross flow. The interactions between the two pipes are modeled by a linear distributed damper, a linear distributed spring and a nonlinear distributed spring along the pipe length. The unsteady hydrodynamic forces due to cross flow are modeled by two distributed van der Pol wake oscillators. The nonlinear partial differential equations for the two pipes and the wake are further discretized by the aid of Galerkin's technique, resulting in a set of ordinary differential equations. These ordinary differential equations are further numerically solved by using a fourth-order Runge–Kutta integration algorithm. Phase portraits, bifurcation diagrams, an Argand diagram and oscillation shape diagrams are plotted, showing the existence of a lock-in phenomenon and figure-of-eight trajectory. The PIP system subjected to cross flow displays some interesting dynamical behaviors different from that of a single-pipe structure.

Keywords Cantilevered PIP structure · Theoretical model · Flow-induced vibration · Cross flow · Internal flow

1 Introduction

Pipe-in-pipe (PIP) structures are widely used in offshore oil and gas pipelines due to their outstanding thermal insulation property. The PIP structures used in offshore industry can be divided into two types [1–5]: (1) fully compliant PIP structures, (2) non-compliant PIP structures. In the case of a fully compliant PIP structure, the whole annulus is filled with insulation materials, and the deformations of inner and outer pipes are completely the same. In the case of a non-compliant PIP structure, the inner pipe is wrapped by insulation pads for insulation, and there may be a relative motion between the inner and outer pipes.

Due to the wide application of PIP systems, the literature on PIP systems has expanded in recent years. The integrity of a PIP system in the event of accidental collapse of the outer pipe was studied by Kyriakides [6] using an experimental method. The experimental results demonstrated that the outer pipe will generate a propagating collapse for any external pressure higher than the propagation pressure of the outer pipe with a solid rod insert. It was shown that, in most cases, the collapse of the outer pipe could lead to another collapse of the inner pipe. In a special case, an interesting phenomenon in which the outer pipe collapses, leaving the inner pipe intact, may occur. The property of three models for estimating the two propagating collapses reported by Kyriakides [6] was further evaluated by Kyriakides and Vogler [7]. The numerical simulation results of the models agreed well with experimental results with acceptable engineering accuracy. Experiments and large-scale numerical simulations on the dynamics and the suppression of buckling propagation in PIP systems were conducted by Kyriakides and Netto [8]. It was observed from their experimental results that the quasi-static controlling

✉ L. Wang
wanglindds@mail.hust.edu.cn

¹ Department of Mechanics, Huazhong University of Science and Technology, Wuhan 430074, China

² Hubei Key Laboratory for Engineering Structural Analysis and Safety Assessment, Wuhan 430074, China

efficiency was lower than the dynamic one in all cases. The same phenomenon was also obtained by numerical calculations. It was shown that the internal ring buckling controller designed by a quasi-static design criteria should be conservative. A three-dimensional (3D) model was established by Gong and Li [9] to simulate the buckling propagation of experimental samples using the ABAQUS software. The good agreement between numerical and experimental results illustrates that the whole buckling propagation process of PIP systems under external pressure can be accurately predicted by the numerical model proposed. It should be mentioned that all the abovementioned investigations of PIP systems mainly focused on the buckling propagation problems.

It is a common phenomenon that marine riser/pipe structures are always subjected to vortex-induced vibrations (VIVs) due to presence of external cross flow. VIV is one typical type of flow-induced vibration (FIVs) and can lead to decrease of the expected design lifetime and even lead to damage. Therefore, it is of great significance for researchers and engineers to study the VIVs of pipe systems. In many cases, a pipe structure may also contain internal fluid flow. In the presence of internal fluid flow, a slender pipe suffers an axial FIV when the internal fluid velocity becomes high. The axial FIV is another typical type of FIV. In the past decades, indeed, a number of studies on FIVs of the system of a single pipe subjected to both internal and external fluid flows were reported [10–18]. However, the studies on the FIVs of PIP systems were relatively limited. Due to the favorable FIV suppression property and significant advantage in terms of fatigue life span of PIP systems, Yettou et al. [1] proposed a fluid–structure interaction (FSI) model to obtain numerical results. Their numerical results were further compared with experimental results. It was shown that the numerical results achieved using the LS-DYNA arbitrary Lagrangian–Eulerian (ALE) penalty coupling algorithm were of excellent engineering accuracy. Slight modification of the conventional PIP system was undertaken by Bi and Hao [19] with the inner and outer pipes being connected with springs and dashpots. They simplified the PIP structure as a non-conventional tuned mass damper (TMD) system. The springs and dashpots were optimized for the proposed PIP systems. It was shown that the proposed PIP systems can obtain better seismic-induced vibration control [20–22] than that of traditional PIP systems. Using the modified PIP system model suggested by Bi and Hao [19], Matin et al. [23] studied the effectiveness of an optimized PIP system to mitigate VIVs of cylindrical structures, and compared the VIV responses of the optimized PIP system with that of a single-pipe system.

It was demonstrated that the proposed PIP system can dramatically suppress the VIV of offshore cylindrical structures, and hence the optimized PIP system is of significant practical value in offshore engineering application. Very recently, Matin et al. [24] used a 3D two-way FSI analysis to investigate the cross-flow (CF) oscillations of both conventional and optimized PIP systems. First, the reliability of the two-way FSI analysis algorithm was validated by introducing previous experimental and numerical results for one single cylinder. Then, the numerical method was extended to model a PIP system. It was demonstrated that the optimized PIP system can significantly suppress the CF VIV of the system compared with the conventional PIP system. A numerical model was proposed by Yang et al. [25] for VIV assessment of sliding PIP systems. The longitudinal stress range resulting from VIVs was achieved, and the fatigue assessment of the PIP systems was performed in accordance with numerical results.

By reviewing the abovementioned valuable studies of the PIP systems, to the authors' knowledge, the literature on the nonplanar FIVs of a flexible PIP structure is very limited, especially in the case in which the inner pipe is conveying fluid flow. This motivates the current study. Section 2 of this paper presents the mathematical model of a PIP system subjected to both external cross flow and internal axial flow. The equations of motion of the inner and outer pipes and the governing equations for external wake variables are given. These partial differential equations (PDEs) are further discretized by using Galerkin's method, resulting in a set of ordinary differential equations (ODEs). In Sect. 3, the lowest several natural frequencies of the PIP system are calculated and analyzed, and the

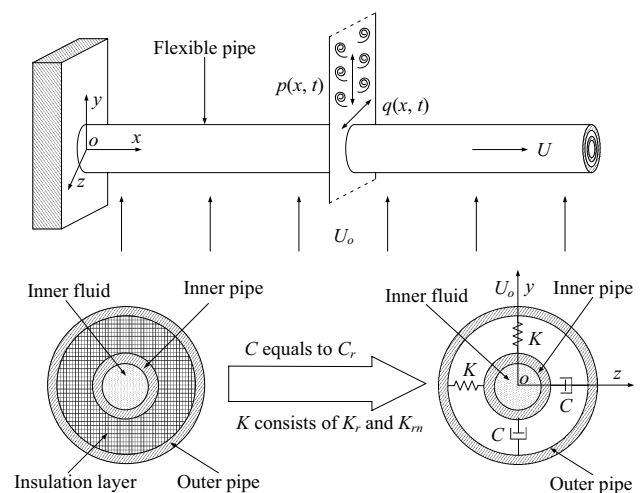


Fig. 1 Schematic of the cantilevered PIP structure system

nonlinear dynamic responses of the PIP system with or without cross flow are investigated. Finally, some conclusions are drawn in Sect. 4.

2 Analytical model and solution

The schematic representation of a horizontal cantilevered PIP system under consideration is depicted in Fig. 1, from where it is seen that y stands for the in-line (IL) direction and z stands for the cross-flow direction. It is assumed that the cantilever is a non-compliant PIP system. The external cross-flow velocity and internal axial-flow velocity are denoted as U_o and U , respectively. In the following analysis, some physical and geometric parameters of the PIP system are selected as: the Young’s modulus of the two pipes $E=210$ GPa, the density of the two pipes $\rho_p=7850$ kg/m³, the density of external fluid $\rho_o=1020$ kg/m³, the density of internal axial fluid $\rho_f=870$ kg/m³ with mass per unit length M . All parameters of the outer pipe are designated by subscript “ o ”, and several key parameters of the outer pipe are selected as: the length $L_o=L=140$ m, the outer diameter $D_o=0.26$ m, the inner diameter $d_o=0.22$ m and the mass per unit length m_o . All parameters of the inner pipe are designated by subscript “ i ”, and several key parameters of the inner pipe are selected as: the length $L_i=L=140$ m, the outer diameter $D_i=0.20$ m, the inner diameter $d_i=0.16$ m and the mass per unit length m_i . The inner and outer pipes are connected by an insulation layer. The effect of the insulation layer may be viewed as a linear damper (C_r) and a nonlinear spring along the pipes’ length [23, 24]. The spring (K) consists of linear component (K_r) and nonlinear component (K_m). The nonlinear component of the spring represents the possible impact force between the two pipes. It was reported by Williams and Kenny [26] that the relative motion could be highly nonlinear as the inner pipe would contact closely with the inner surface of the outer pipe in some cases.

2.1 Governing equations of the inner pipe

For either an inner or outer cantilevered pipe, two variables $v(s, t)$ and $w(s, t)$ stand for the pipe’s lateral displacements along the y and z axes, respectively, with s being the curvilinear coordinate along the length of the pipe and t being the time. In the present work, unless particularly stated, the lateral displacements of the outer pipe are designated by subscript “ o ”, and the lateral displacements of the inner pipe are designated by subscript “ i ”. Following the derivation of Wadham-Gagnon et al. [27] and Liu et al. [28]

and neglecting gravity, the 3D version of the governing equations for the inner pipe may be written as: in the y direction

$$\begin{aligned}
 & (M + m_i)\ddot{v}_i + EI_i v_i'''' + 2MU\dot{v}_i + MU^2 v_i'' \\
 & + C_i \dot{v}_i + K_r(v_i - v_o) \\
 & + 2MU \left[\dot{v}_i v_i'^2 + v_i' w_i' \dot{w}_i' - v_i'' \int_s^L (v_i' \dot{v}_i' + w_i' \dot{w}_i') ds \right] \\
 & + C_r(\dot{v}_i - \dot{v}_o) - (M + m_i)v_i'' \int_s^L \int_0^s (\dot{v}_i'^2 \\
 & + v_i' \dot{v}_i' + \dot{w}_i'^2 + w_i' \dot{w}_i') ds ds + MU^2 (v_i'' v_i'^2 + v_i' w_i' w_i'') \\
 & + K_m \left[R - \frac{1}{2} (|R + R_b| - |R - R_b|) \right]^3 \frac{v_i - v_o}{R} \\
 & - MU^2 v_i'' \int_s^L (v_i' v_i'' + w_i' w_i'') ds \\
 & + (M + m_i)v_i' \int_0^s (\dot{v}_i'^2 + v_i' \dot{v}_i' + \dot{w}_i'^2 + w_i' \dot{w}_i') ds \\
 & + EI_i (v_i'''' v_i'^2 + v_i''^3 + 4v_i' v_i'' v_i''' + v_i'' w_i''^2 \\
 & + v_i'' w_i' w_i''' + 3v_i' w_i'' w_i''' + v_i' w_i' w_i'''') = 0, \tag{1}
 \end{aligned}$$

in the z direction

$$\begin{aligned}
 & (M + m_i)\ddot{w}_i + EI_i w_i'''' + 2MU\dot{w}_i + MU^2 w_i'' \\
 & + C_i \dot{w}_i + K_r(w_i - w_o) \\
 & + 2MU \left[\dot{w}_i w_i'^2 + w_i' v_i' \dot{v}_i' - w_i'' \int_s^L (w_i' \dot{w}_i' + v_i' \dot{v}_i') ds \right] \\
 & + C_r(\dot{w}_i - \dot{w}_o) \\
 & - (M + m_i)w_i'' \int_s^L \int_0^s (\dot{w}_i'^2 + w_i' \dot{w}_i' + \dot{v}_i'^2 + v_i' \dot{v}_i') ds ds \\
 & + MU^2 (w_i'' w_i'^2 + w_i' v_i' v_i'') \\
 & + K_m \left[R - \frac{1}{2} (|R + R_b| - |R - R_b|) \right]^3 \frac{w_i - w_o}{R} \\
 & - MU^2 w_i'' \int_s^L (w_i' w_i'' + v_i' v_i'') ds \\
 & + (M + m_i)w_i' \int_0^s (\dot{w}_i'^2 + w_i' \dot{w}_i' + \dot{v}_i'^2 + v_i' \dot{v}_i') ds \\
 & + EI_i (w_i'''' w_i'^2 + w_i''^3 + 4w_i' w_i'' w_i''' + w_i'' v_i''^2 \\
 & + w_i'' v_i' v_i''' + 3w_i' v_i'' v_i''' + w_i' v_i' v_i'''') = 0, \tag{2}
 \end{aligned}$$

where R denotes the relative motion displacement between the inner and outer pipes and is given by $R = \sqrt{(w_i - w_o)^2 + (v_i - v_o)^2}$, and R_b is the initial gap between the inner and outer pipes; the prime and overdot on each variable stand for the derivative with respect to s and t , respectively.

Equations (1) and (2) can be transformed into a dimensionless form through the use of

$$\xi = \frac{s}{L}, \quad \eta = \frac{v}{L}, \quad \zeta = \frac{w}{L}, \quad \tau = \left(\frac{EI_i}{m_i + M} \right)^{1/2} \frac{t}{L^2},$$

$$u = \left(\frac{M}{EI_i} \right)^{1/2} UL, \quad c_r = \frac{C_r L^2}{EI_i(M + m_i)^{1/2}}, \quad \beta = \frac{M}{M + m_i},$$

$$c_i = \frac{C_i L^2}{EI_i(M + m_i)^{1/2}}, \quad k_r = \frac{K_r L^4}{EI_i}, \quad k_{rm} = \frac{K_{rm} L^6}{EI_i},$$

where u is the dimensionless fluid velocity of the internal axial flow.

The dimensionless equations are

$$\begin{aligned} & \ddot{\eta}_i + 2\sqrt{\beta}u\dot{\eta}'_i + \eta_i'''' + u^2\eta_i'' \\ & + 2\sqrt{\beta}u(\eta_i''\dot{\eta}'_i + \eta_i'\dot{\zeta}'_i) + c_i\dot{\eta}_i \\ & + u^2(\eta_i''\eta_i'' + \eta_i'\zeta_i''') + \eta_i''^3 + 3\eta_i'\eta_i''\eta_i'''' \\ & + \eta_i''\zeta_i''^2 + c_r(\dot{\eta}_i - \dot{\eta}_o) + k_r(\eta_i - \eta_o) \\ & + k_{rm}\left[r - \frac{1}{2}(|r + r_b| - |r - r_b|)\right]^3 \frac{(\eta_i - \eta_o)}{r} \\ & + 3\eta_i'\zeta_i''\zeta_i'''' - \eta_i'' \int_{\xi}^1 \left[2\sqrt{\beta}u\eta_i'\dot{\eta}'_i + u^2\eta_i''\eta_i'' + \eta_i''\eta_i'''' \right. \\ & \left. + 2\sqrt{\beta}u\zeta_i'\dot{\zeta}'_i + u^2\zeta_i'\zeta_i'' + \zeta_i''\zeta_i'''' \right] d\xi \\ & + \eta_i' \int_0^{\xi} \left[\begin{aligned} & \dot{\eta}_i^2 - 2\sqrt{\beta}u\eta_i'\dot{\eta}'_i - u^2\eta_i''\eta_i'' + \eta_i''\eta_i'''' - \\ & c_i\eta_i'\dot{\eta}'_i - k_r\eta_i'(\eta_i' - \eta_o') - c_r\eta_i'(\dot{\eta}'_i - \dot{\eta}'_o) \\ & + \dot{\zeta}_i^2 - 2\sqrt{\beta}u\zeta_i'\dot{\zeta}'_i - u^2\zeta_i'\zeta_i'' + \zeta_i''\zeta_i'''' - \\ & c_i\zeta_i'\dot{\zeta}'_i - k_r\zeta_i'(\zeta_i' - \zeta_o') - c_r\zeta_i'(\dot{\zeta}'_i - \dot{\zeta}'_o) \end{aligned} \right] d\xi \\ & - \eta_i'' \int_{\xi}^1 \int_0^{\xi} \left[\begin{aligned} & \dot{\eta}_i^2 - 2\sqrt{\beta}u\eta_i'\dot{\eta}'_i - u^2\eta_i''\eta_i'' + \eta_i''\eta_i'''' - \\ & c_i\eta_i'\dot{\eta}'_i - k_r\eta_i'(\eta_i' - \eta_o') - c_r\eta_i'(\dot{\eta}'_i - \dot{\eta}'_o) \\ & + \dot{\zeta}_i^2 - 2\sqrt{\beta}u\zeta_i'\dot{\zeta}'_i - u^2\zeta_i'\zeta_i'' + \zeta_i''\zeta_i'''' - \\ & c_i\zeta_i'\dot{\zeta}'_i - k_r\zeta_i'(\zeta_i' - \zeta_o') - c_r\zeta_i'(\dot{\zeta}'_i - \dot{\zeta}'_o) \end{aligned} \right] d\xi d\xi = 0, \end{aligned} \tag{3}$$

$$\begin{aligned} & \ddot{\zeta}_i + 2\sqrt{\beta}u\dot{\zeta}'_i + \zeta_i'''' + u^2\zeta_i'' + 2\sqrt{\beta}u(\zeta_i''\dot{\zeta}'_i + \zeta_i'\dot{\eta}'_i) + c_i\dot{\zeta}_i \\ & + u^2(\zeta_i''\zeta_i'' + \zeta_i'\eta_i''') + \zeta_i''^3 + 3\zeta_i'\zeta_i''\zeta_i'''' + \zeta_i''\eta_i''^2 + c_r(\dot{\zeta}_i - \dot{\zeta}_o) \\ & + k_r(\zeta_i - \zeta_o) + k_{rm}\left(r - \frac{1}{2}(|r + r_b| - |r - r_b|)\right)^3 \frac{(\zeta_i - \zeta_o)}{r} \\ & + 3\zeta_i'\eta_i''\eta_i'''' - \zeta_i'' \int_{\xi}^1 \left(2\sqrt{\beta}u\eta_i'\dot{\eta}'_i + u^2\eta_i''\eta_i'' + \eta_i''\eta_i'''' \right. \\ & \left. + 2\sqrt{\beta}u\zeta_i'\dot{\zeta}'_i + u^2\zeta_i'\zeta_i'' + \zeta_i''\zeta_i'''' \right) d\xi \\ & + \zeta_i' \int_0^{\xi} \left[\begin{aligned} & \dot{\eta}_i^2 - 2\sqrt{\beta}u\eta_i'\dot{\eta}'_i - u^2\eta_i''\eta_i'' + \eta_i''\eta_i'''' - \\ & c_i\eta_i'\dot{\eta}'_i - k_r\eta_i'(\eta_i' - \eta_o') - c_r\eta_i'(\dot{\eta}'_i - \dot{\eta}'_o) \\ & + \dot{\zeta}_i^2 - 2\sqrt{\beta}u\zeta_i'\dot{\zeta}'_i - u^2\zeta_i'\zeta_i'' + \zeta_i''\zeta_i'''' - \\ & c_i\zeta_i'\dot{\zeta}'_i - k_r\zeta_i'(\zeta_i' - \zeta_o') - c_r\zeta_i'(\dot{\zeta}'_i - \dot{\zeta}'_o) \end{aligned} \right] d\xi \\ & - \zeta_i'' \int_{\xi}^1 \int_0^{\xi} \left[\begin{aligned} & \dot{\eta}_i^2 - 2\sqrt{\beta}u\eta_i'\dot{\eta}'_i - u^2\eta_i''\eta_i'' + \eta_i''\eta_i'''' - \\ & c_i\eta_i'\dot{\eta}'_i - k_r\eta_i'(\eta_i' - \eta_o') - c_r\eta_i'(\dot{\eta}'_i - \dot{\eta}'_o) \\ & + \dot{\zeta}_i^2 - 2\sqrt{\beta}u\zeta_i'\dot{\zeta}'_i - u^2\zeta_i'\zeta_i'' + \zeta_i''\zeta_i'''' - \\ & c_i\zeta_i'\dot{\zeta}'_i - k_r\zeta_i'(\zeta_i' - \zeta_o') - c_r\zeta_i'(\dot{\zeta}'_i - \dot{\zeta}'_o) \end{aligned} \right] d\xi d\xi = 0, \end{aligned} \tag{4}$$

where the prime and overdot on each variable now denote the derivative with respect to ξ and τ , respectively.

2.2 Governing equations of the outer pipe

Following the derivation of Wadham-Gagnon et al. [27] and Liu et al. [28], the 3D version of the governing equations for the outer pipe may be written as:

in the y direction

$$\begin{aligned} & (m_o + m_a)\ddot{v}_o + EI_o v_o'''' + C_o \dot{v}_o \\ & + (m_o + m_a)v_o' \int_0^s (\dot{v}_o'^2 + v_o' \ddot{v}_o' + \dot{w}_o'^2 + w_o' \ddot{w}_o') ds \\ & - (m_o + m_a)v_o'' \int_s^L \int_0^s (\dot{v}_o'^2 + v_o' \ddot{v}_o' + \dot{w}_o'^2 + w_o' \ddot{w}_o') ds ds \\ & + K_r(v_o - v_i) + C_r(\dot{v}_o - \dot{v}_i) \\ & + K_{rm}\left[R - \frac{1}{2}(|R + R_b| - |R - R_b|)\right]^3 \frac{v_o - v_i}{R} \\ & + EI_o(v_o'''' v_o'^2 + v_o''^2 + 4v_o' v_o'' v_o'''' + v_o'' w_o''^2 \\ & + v_o'' w_o' w_o'''' + 3v_o' w_o'' w_o'''' + v_o' w_o' w_o''''') = F_y, \end{aligned} \tag{5}$$

in the z direction

$$\begin{aligned} & (m_o + m_a)\ddot{w}_o + EI_o w_o'''' + C_o \dot{w}_o \\ & + (m_o + m_a)w_o' \int_0^s (\dot{w}_o'^2 + w_o' \ddot{w}_o' + \dot{v}_o'^2 + v_o' \ddot{v}_o') ds \\ & - (m_o + m_a)w_o'' \int_s^L \int_0^s (\dot{w}_o'^2 + w_o' \ddot{w}_o' + \dot{v}_o'^2 + v_o' \ddot{v}_o') ds ds \\ & + K_r(w_o - w_i) + C_r(\dot{w}_o - \dot{w}_i) \\ & + K_{rm}\left[R - \frac{1}{2}(|R + R_b| - |R - R_b|)\right]^3 \frac{w_o - w_i}{R} \\ & + EI_o(w_o'''' w_o'^2 + w_o''^3 + 4w_o' w_o'' w_o'''' + w_o'' v_o''^2 \\ & + w_o'' v_o' v_o'''' + 3w_o' v_o'' v_o'''' + w_o' v_o' v_o''''') = F_z, \end{aligned} \tag{6}$$

where the prime and overdot on each variable stand for the derivative with respect to s and t , respectively.

The damping coefficient C_o of the outer pipe consists of a viscous dissipation in the structure c_s and a fluid-added damping c_f , while the damping coefficient C_i of the inner pipe just depends on a viscous dissipation in the structure [29], thus we have

$$C_o = c_s + c_f = 2\chi(m_o + m_a)\Omega_r + \vartheta\Omega_s\rho_o D_o^2, \quad C_i = 2\chi(M + m_i)\Omega_r, \tag{7}$$

where Ω_r is the angular frequency of the pipe, χ is the structural damping ratio, ϑ is a stall parameter usually estimated using experiment data, as discussed in Refs. [30, 31]. The two key parameters in Eq. (7) will be chosen as: $\chi=0.001$ and $\vartheta=0.8$. In Eq. (7), Ω_s is the vortex shedding angular frequency. In addition, the added fluid mass m_a per unit length is assumed to be independent of time and is given by

$$m_a = \frac{\pi}{4} C_a \rho_0 D_o^2, \tag{8}$$

where C_a is the added mass coefficient, and is chosen to be 1 for cylindrical structures as reported by Munir et al. [32] and Yang et al. [33].

The external hydrodynamic force, F_y and F_z are induced by the wake dynamics and may be expressed as [31]

$$F_y = f_D + f_{D0} - \frac{f_L}{U_o} \frac{\partial w}{\partial t}, F_z = f_L + \frac{f_D}{U_o} \frac{\partial w}{\partial t}, \tag{9}$$

in which f_D is the vortex-induced fluctuating drag force, f_{D0} is the average drag force, and f_L is the lift force exerted on the outer pipe. The two drag forces and the lift force are given by [31]

$$f_D = \frac{1}{2} C_{Di} \rho_0 D_o U_o^2, f_{D0} = \frac{1}{2} C_{D0} \rho_0 D_o U_o^2, f_L = \frac{1}{2} C_L \rho_0 D_o U_o^2 \tag{10}$$

where C_{Di} is a vortex-induced drag term depending on time, C_{D0} is the drag coefficient for a pipe at rest, and C_L is the lift coefficient. In the present study, C_{Di} and C_L will be written as

$$C_{Di} = C_{D0i} \frac{p}{2}, C_L = C_{L0} \frac{q}{2}, \tag{11}$$

where p and q are the vortex wake variables in the y and z directions, respectively; C_{D0i} and C_{L0} are the corresponding unsteady drag and lift coefficients of a stationary pipe subjected to shedding vortex. In this work, a set of system parameter values are set as [29, 30]: $C_{D0i}=0.1$, $C_{D0}=2$ and $C_{L0}=0.3$.

Equations (5) and (6) can be transformed into dimensionless form through the use of

$$\begin{aligned} \xi &= \frac{s}{L}, \quad \eta = \frac{v}{L}, \quad \zeta = \frac{w}{L}, \quad \theta = \frac{L}{D_o}, \\ \tau &= \left(\frac{EI_i}{m_i + M} \right)^{1/2} \frac{t}{L^2}, \quad \alpha_1 = \frac{EI_o}{EI_i}, \\ c_r &= \frac{C_r L^2}{[EI_i(M + m_i)]^{1/2}}, \quad k_r = \frac{K_r L^4}{EI_i}, \\ \omega_s &= \Omega_s \sqrt{\frac{m_i + M}{EI_i}} L^2, \quad \alpha_2 = \frac{m_a + m_o}{M + m_i}, \\ c_o &= \frac{C_o L^2}{[EI_i(M + m_i)]^{1/2}}, \quad k_m = \frac{K_m L^6}{EI_i}, \\ \alpha &= \frac{\rho_0 U_o^2 D_o L^3}{4 EI_i}, \quad \zeta = \frac{\rho_0 U_o D_o L^2}{4 \sqrt{(M + m_i) EI_i}}. \end{aligned}$$

The dimensionless forms of Eqs. (5) and (6) are

$$\begin{aligned} &\alpha_2 \ddot{\eta}_o + \alpha_1 (\eta_o'''' + \eta_o''' + 3\eta_o' \eta_o'' \eta_o'''' + \eta_o'' \zeta_o''^2 + 3\eta_o' \zeta_o'' \zeta_o'''') \\ &+ k_r (\eta_o - \eta_i) - \alpha_1 \eta_o'' \int_{\xi}^1 (\eta_o'' \eta_o'''' + \zeta_o'' \zeta_o'''') d\xi \\ &+ k_m \left[r - \frac{1}{2} (|r + \eta_b| - |r - \eta_b|) \right]^3 \frac{(\eta_o - \eta_i)}{r} \\ &+ \eta_o' \int_0^{\xi} \left[\begin{aligned} &\alpha_2 \dot{\eta}_o'' + \alpha_1 \eta_o'' \eta_o'''' - c_o \eta_o' \dot{\eta}_o' + \alpha C_{D0i} \eta_o' p' \\ &- k_r \eta_o' (\eta_o' - \eta_i') - c_r \eta_o' (\dot{\eta}_o' - \dot{\eta}_i') \\ &+ \alpha_2 \dot{\zeta}_o'' + \alpha_1 \zeta_o'' \zeta_o'''' - c_o \zeta_o' \dot{\zeta}_o' + \alpha C_{L0} \zeta_o' q' \\ &- k_r \zeta_o' (\zeta_o' - \zeta_i') - c_r \zeta_o' (\dot{\zeta}_o' - \dot{\zeta}_i') \end{aligned} \right] d\xi \\ &- \eta_o'' \int_{\xi}^1 \int_0^{\xi} \left[\begin{aligned} &\alpha_2 \dot{\eta}_o'' + \alpha_1 \eta_o'' \eta_o'''' - c_o \eta_o' \dot{\eta}_o' + \alpha C_{D0i} \eta_o' p' \\ &- k_r \eta_o' (\eta_o' - \eta_i') - c_r \eta_o' (\dot{\eta}_o' - \dot{\eta}_i') \\ &+ \alpha_2 \dot{\zeta}_o'' + \alpha_1 \zeta_o'' \zeta_o'''' - c_o \zeta_o' \dot{\zeta}_o' + \alpha C_{L0} \zeta_o' q' \\ &- k_r \zeta_o' (\zeta_o' - \zeta_i') - c_r \zeta_o' (\dot{\zeta}_o' - \dot{\zeta}_i') \end{aligned} \right] d\xi d\xi \\ &- 2\alpha C_{D0} - \alpha C_{D0i} p + \zeta C_{L0} q \zeta_o + c_o \dot{\eta}_o + c_r (\dot{\eta}_o - \dot{\eta}_i) = 0, \tag{12} \end{aligned}$$

$$\begin{aligned} &\alpha_2 \ddot{\zeta}_o + \alpha_1 (\zeta_o'''' + \zeta_o''' + 3\zeta_o' \zeta_o'' \zeta_o'''' + \zeta_o'' \eta_o''^2 + 3\zeta_o' \eta_o'' \eta_o'''') \\ &+ k_r (\zeta_o - \zeta_i) - \alpha_1 \zeta_o'' \int_{\xi}^1 (\eta_o'' \eta_o'''' + \zeta_o'' \zeta_o'''') d\xi \\ &+ k_m \left[r - \frac{1}{2} (|r + \eta_b| - |r - \eta_b|) \right]^3 \frac{(\zeta_o - \zeta_i)}{r} \\ &+ \zeta_o' \int_0^{\xi} \left[\begin{aligned} &\alpha_2 \dot{\eta}_o'' + \alpha_1 \eta_o'' \eta_o'''' - c_o \eta_o' \dot{\eta}_o' + \alpha C_{D0i} \eta_o' p' \\ &- k_r \eta_o' (\eta_o' - \eta_i') - c_r \eta_o' (\dot{\eta}_o' - \dot{\eta}_i') \\ &+ \alpha_2 \dot{\zeta}_o'' + \alpha_1 \zeta_o'' \zeta_o'''' - c_o \zeta_o' \dot{\zeta}_o' + \alpha C_{L0} \zeta_o' q' \\ &- k_r \zeta_o' (\zeta_o' - \zeta_i') - c_r \zeta_o' (\dot{\zeta}_o' - \dot{\zeta}_i') \end{aligned} \right] d\xi \\ &- \zeta_o'' \int_{\xi}^1 \int_0^{\xi} \left[\begin{aligned} &\alpha_2 \dot{\eta}_o'' + \alpha_1 \eta_o'' \eta_o'''' - c_o \eta_o' \dot{\eta}_o' + \alpha C_{D0i} \eta_o' p' \\ &- k_r \eta_o' (\eta_o' - \eta_i') - c_r \eta_o' (\dot{\eta}_o' - \dot{\eta}_i') \\ &+ \alpha_2 \dot{\zeta}_o'' + \alpha_1 \zeta_o'' \zeta_o'''' - c_o \zeta_o' \dot{\zeta}_o' + \alpha C_{L0} \zeta_o' q' \\ &- k_r \zeta_o' (\zeta_o' - \zeta_i') - c_r \zeta_o' (\dot{\zeta}_o' - \dot{\zeta}_i') \end{aligned} \right] d\xi d\xi \\ &- \alpha C_{L0} q - \zeta C_{D0i} p \zeta_o + c_o \dot{\zeta}_o + c_r (\dot{\zeta}_o - \dot{\zeta}_i) = 0, \tag{13} \end{aligned}$$

where the prime and overdot on each variable stand for the derivative with respect to ξ and τ , respectively.

The dimensionless equations of the wake oscillators are given by Wang et al. [29]

$$\begin{aligned} \ddot{q} + \omega_s \varepsilon_z (q^2 - 1) \dot{q} + \omega_s^2 q &= \theta \Lambda_z \ddot{\zeta}, \\ \ddot{p} + 2\omega_s \varepsilon_y (p^2 - 1) \dot{p} + 4\omega_s^2 p &= \theta \Lambda_y \ddot{\eta}, \end{aligned} \tag{14}$$

in which a set of system parameter values are set as [29] $\varepsilon_y=0.02$, $\varepsilon_z=0.04$, $\Lambda_y=96$, $\Lambda_z=12$.

2.3 Solution method

It is seen that the governing equations for the PIP system and wake are in partial differential form. Galerkin's method will be used to solve Eqs. (3), (4), (12)–(14). According to this method, the oscillation displacements of the inner and outer pipes and the wake variables can be given by

$$\begin{aligned} \eta_i(\xi, \tau) &= \sum_{r=1}^{\infty} \varphi_r(\xi) \bar{\eta}_i(\tau), & \zeta_i(\xi, \tau) &= \sum_{r=1}^{\infty} \varphi_r(\xi) \bar{\zeta}_i(\tau), \\ \eta_o(\xi, \tau) &= \sum_{r=1}^{\infty} \varphi_r(\xi) \bar{\eta}_o(\tau), & \zeta_o(\xi, \tau) &= \sum_{r=1}^{\infty} \varphi_r(\xi) \bar{\zeta}_o(\tau), \\ p(\xi, \tau) &= \sum_{r=1}^{\infty} \varphi_r(\xi) \bar{p}_r(\tau), & q(\xi, \tau) &= \sum_{r=1}^{\infty} \varphi_r(\xi) \bar{q}_r(\tau), \end{aligned} \quad (15)$$

where $\varphi_r(\xi)$ is the dimensionless eigenfunctions of a cantilevered beam, $\bar{\eta}_o(\tau)$ and $\bar{p}_r(\tau)$ are the corresponding generalized coordinates of the outer pipe in the y direction, $\bar{\zeta}_o(\tau)$ and $\bar{q}_r(\tau)$ are the corresponding generalized coordinates of the outer pipe in the z direction, and $\bar{\eta}_i(\tau)$ and $\bar{\zeta}_i(\tau)$ are the corresponding generalized coordinates of the inner pipe in the y and z directions, respectively. It should be noted that the series Eq. (15) can be truncated at a reasonably large value of r (i.e. $r=N$). Since Galerkin's method has been extensively used for studying the nonlinear vibrations of pipes conveying fluid [34–38]), the PDEs of the PIP system coupled with cross flow will be discretized with the aid of Galerkin's method without giving any additional details of this method.

3 Results and discussion

In this section, the main aim is to investigate the FIVs of the PIP system based on numerical calculations. For that purpose, the reduced cross-flow velocities are varied in the range of $0 \leq U_r \leq 50$, where U_r is defined as $U_r = 2\pi U_o / (\Omega_1 D)$, with Ω_1 being the first-order natural frequency of the PIP system for a given internal fluid velocity [39]. In this range of reduced cross-flow velocities, extensive calculations indicate that the dynamic responses of the PIP are only dominated by the lowest several modes of the system. Thus, the nonlinear partial differential Eqs. (3), (4) and (12)–(14) are discretized via Galerkin's method with a five-mode truncation. The obtained high-dimensional, reduced-order PDEs will be further numerically solved by using a fourth-order Runge–Kutta integration algorithm. The numerical results are plotted in the form of phase portraits, bifurcation diagrams, Argand diagram and oscillation shape diagrams, to show the various dynamical behaviors of the PIP system. In the present study, the three key dimensionless parameters of the insulation layer are set as: $k_r=100$, $k_m=1 \times 10^{13}$, and $c_r=0.2$.

3.1 Validation of the proposed model

Owing to the lack of FIV experiments on cantilevered fluid-conveying PIP structures, the validation of the proposed model will be performed using a typical apparatus of a single-pipe structure designed by Song et al. [40].

To check the accuracy of the calculation procedure, the validation example for our analytical model is a pinned–pinned pipe containing internal fluid and subjected to external cross flow. The experiment of VIVs of this pipe

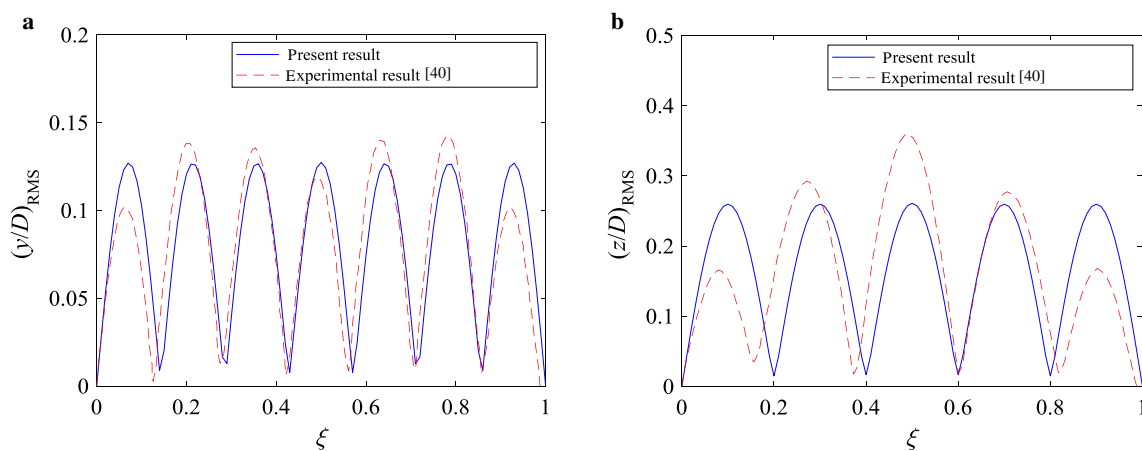


Fig. 2 Distributions of RMS displacements along the flexible riser length with a uniform cross flow of $U_o=2.8$ m/s for **a** in-line direction and **b** cross-flow direction

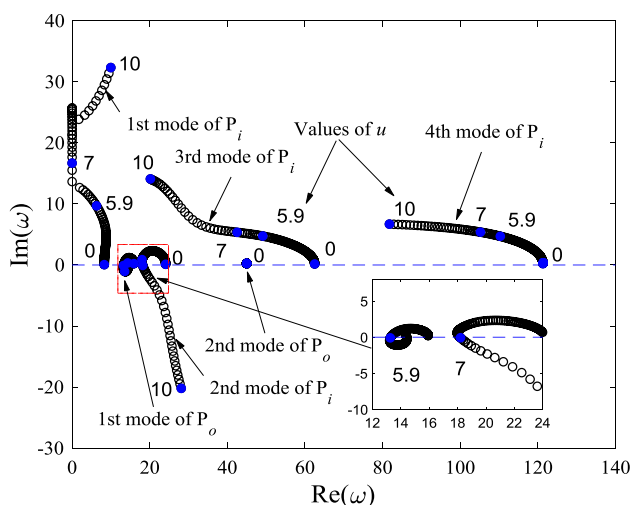


Fig. 3 Argand diagram for the cantilevered PIP structure system without cross flow

structure was conducted by Song et al. [40]. For comparison purposes, all the system parameters were chosen to be the same as those utilized by Song et al. [40]: the pipe length $L=7.9$ m, the outer diameter $D=0.03$ m, the inner diameter $d=0.027$ m, the Young’s modulus $E=108$ GPa, the bending stiffness $EI=1476.63$ N·m², the mass per unit length of the pipe $m=1.768$ kg/m, the mass ratio $m^*=2.5$ and the pretension $T=2943$ N.

The distributions of root mean square (RMS) displacements for the flexible riser under cross flow ($U_o=2.8$ m/s) are shown in Fig. 2. In this figure, the red dash line stands for the experimental result reported by Song et al. [40], while the blue solid line stands for the predicted result based on our proposed model. It is obvious that the present result has an acceptable agreement with experimental data [40].

3.2 Basic dynamics of the cantilevered PIP structure system in the absence of cross flow

The Argand diagram of a cantilevered PIP structure system is plotted in Fig. 3, which greatly different from that of a single cantilevered pipe system. In Fig. 3, the abbreviations P_i and P_o correspond to the inner pipe and outer pipe, respectively. In Fig. 3, the evolution of the lowest four non-dimensional eigen-frequencies of the inner pipe, and the evolution of the lowest two non-dimensional eigen-frequencies of the outer pipe with increasing internal flow velocity are shown. The purpose of a smaller region of the figure is to show the critical flow velocity more clearly. It is immediately seen that the evolution of the lowest four non-dimensional eigen-frequencies of the inner pipe is qualitatively similar to that of one single pipe [28]. It is interesting that, for the outer pipe, only the first-mode eigen-frequency is affected due to the presence of the inner pipe and the insulation layer. It is found that the flutter instability of the outer pipe occurs at about $u=5.9$, and that of the inner pipe occurs at about $u=7.0$, as shown in Fig. 3. It is obvious that the two critical internal flow velocities of the PIP system ($u_{cr}=5.9$ and 7.0) are larger than that of single-pipe system ($u_{cr}=5.3$) as reported by Liu et al. [28]. That is to say, the additional outer pipe and insulation layer can enhance the stability of the original single pipe conveying fluid to a certain extent.

The bifurcation diagrams of the outer pipe at $\xi=1$ without cross flow are shown in Fig. 4. It is seen from Fig. 4 that, for a given u beyond the lowest critical flow velocity ($u_{cr}=5.9$) of the outer pipe, the displacement amplitudes at the free end of the outer pipe increase slowly with increasing u . Such a slow increase of oscillation amplitude with increasing internal flow velocity may be due to the fact that the inner pipe is still stable for $5.9 < u < 7.0$. For a given u beyond the secondary critical flow velocity ($u_{cr}=7.0$) of the inner pipe, however, the displacement amplitudes at the free end of the outer pipe

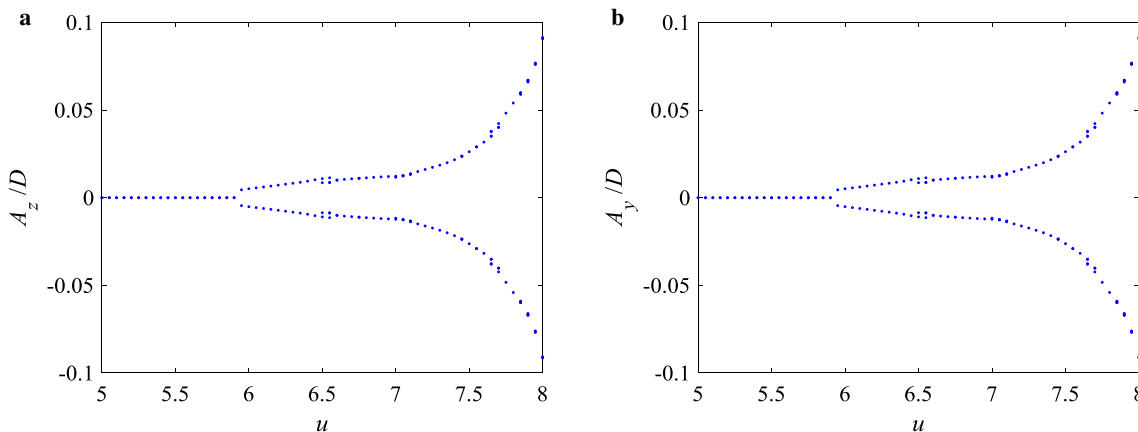


Fig. 4 Bifurcation diagrams of the outer pipe at $\xi=1$ without cross flow for **a** z direction and **b** y direction

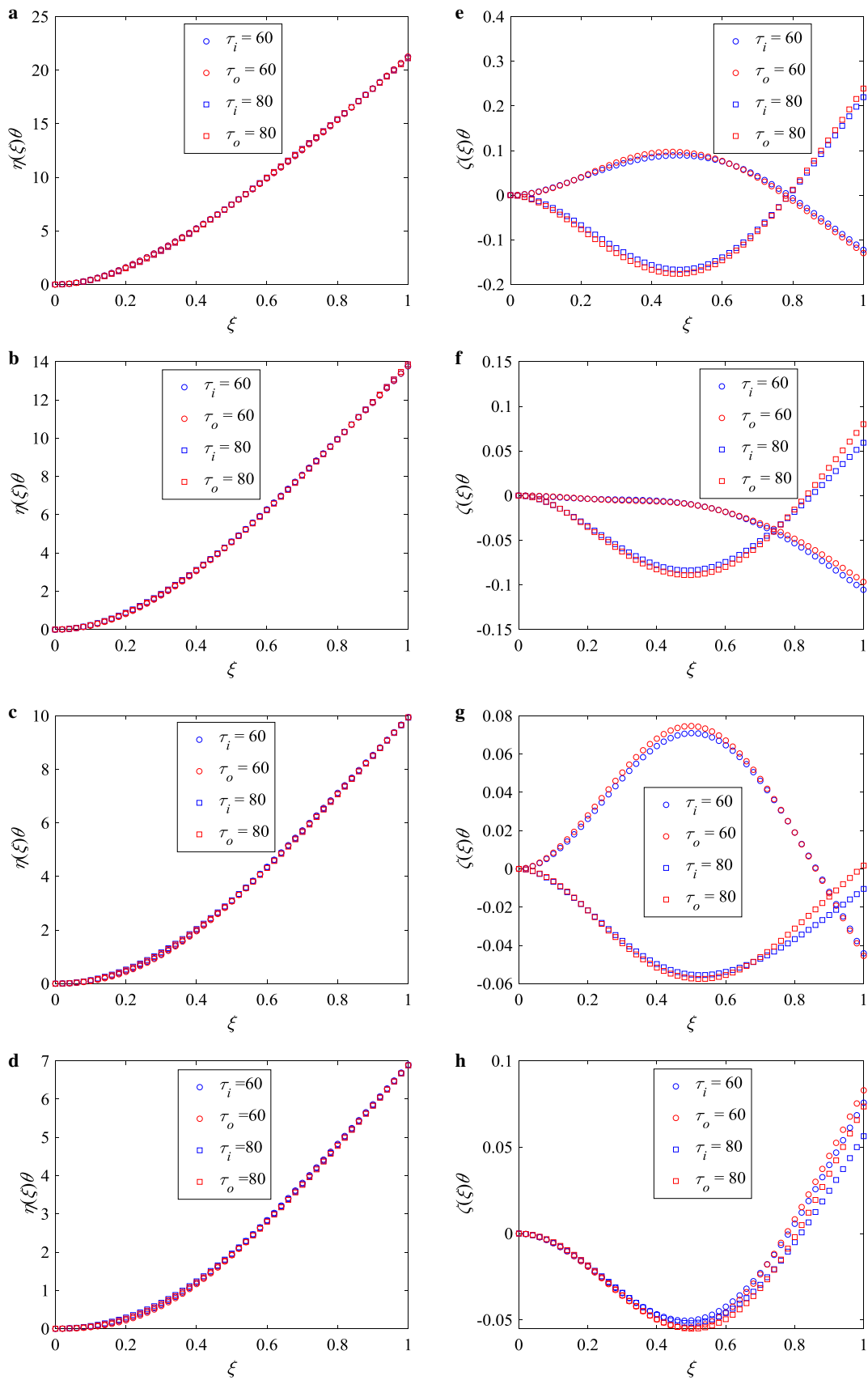


Fig. 5 Comparison of the oscillation shapes of the inner and outer pipes at the time of $\tau=60$ and $\tau=80$ for $U_r=44$, **a, e** in-line and cross-flow responses for $u=0$, respectively; **b, f** in-line and cross-flow responses for $u=5$, respectively; **c, g** in-line and cross-flow responses for $u=6.6$, respectively; **d, h** in-line and cross-flow responses for $u=8$, respectively

increase exponentially. Such a sharp increasing trend of oscillation amplitude with increasing internal flow velocity is due to the fact that both inner and outer pipes are unstable for $u > 7.0$.

3.3 Nonlinear FIV responses of the cantilevered PIP structure system for varied U_r and several typical values of u

In the current work, a non-compliant PIP system will be considered. It has been demonstrated by Bokaian [41] and Wang [42] that there is relative motion between the inner and outer pipes in such a non-compliant PIP system. In this section, the results shown in Fig. 5 are the oscillation shapes of the inner and outer pipes at the time of $\tau=60$ and $\tau=80$ for four typical values of u . In this figure, the circles stand

for the responses of the PIP system at the time of $\tau=60$, and the squares stand for the responses of the PIP system at the time of $\tau=80$. Moreover, the oscillations of the inner pipe are designated by subscript “ i ”, and those of the outer pipe are designated by subscript “ o ”. Figure 5a–d shows the in-line (IL) oscillation shapes of the inner and outer pipes. It is obvious that the inner and outer pipes keep the same oscillation shape for $\tau=60$ or $\tau=80$. Moreover, the inner and outer pipes keep the same cross-flow oscillation shapes for a given time, as shown in Fig. 5e–h. Furthermore, it is obvious that the relative displacements between the outer and inner pipes are smaller than the clearance between the outer and inner pipes.

Figure 6 shows the oscillation shape of the PIP system for $u=0$ and $U_r=44$. The results shown in Fig. 6a, b correspond to the CF responses of the outer pipe and the inner pipe, respectively. The outer and inner pipes are of the same CF oscillation shapes, and they are mainly dominated by the second mode. Moreover, the outer and inner pipes are of the same IL oscillation shapes dominated by the third mode with almost the same amplitude, as shown in Fig. 6c, d.

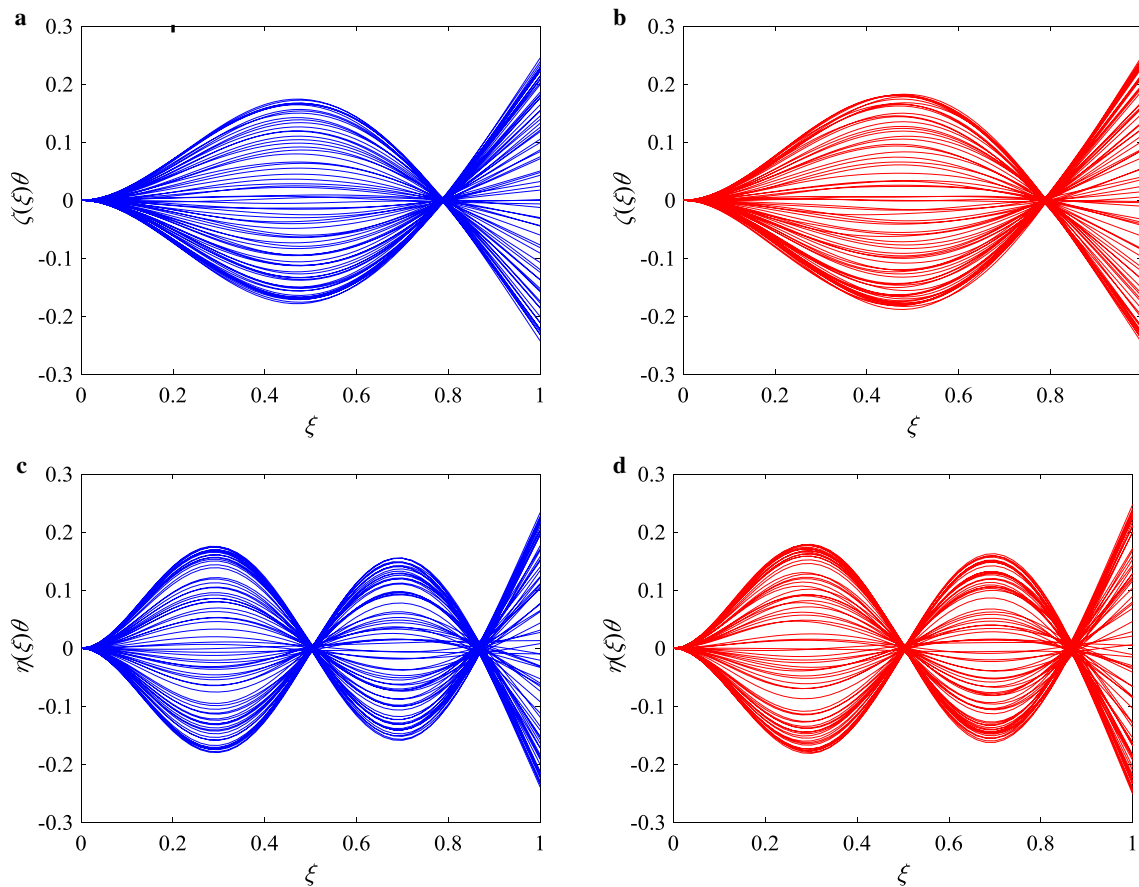


Fig. 6 Oscillation shapes of the PIP system for $U_r = 44$ and $u=0$: **a, b** cross flow motions of the outer and inner pipes, respectively; **c, d** in-line motions with removal of the mean values of the outer and inner pipes, respectively

The oscillation shapes of the PIP system for $U_r=44$ with a subcritical internal flow velocity $u=5$ are shown in Fig. 7. Similar results for $U_r=44$ with a supercritical internal flow velocity $u=8$ are shown in Fig. 8. As can be seen in Figs. 7 and 8, the CF oscillation shapes of the outer and inner pipes are mainly dominated by the second mode, while the IL oscillation shapes of the outer and inner pipes are mainly dominated by the third mode. In both figures, it is seen that the oscillation responses of the outer and inner pipes have almost the same oscillation shapes and amplitudes. Actually, the motions of the outer and inner pipes are almost synchronous. Due to this fact, only the results of the outer pipe have been presented in Fig. 4, and in the following discussion, only the dynamic responses of the outer pipe will be focused.

Some further numerical results presented in the form of bifurcation diagrams are concerned with the possible dynamical behavior of the PIP system subjected to cross flow. Several bifurcation diagrams for the IL or CF displacements at the tip end of the outer pipe are plotted in Fig. 9. Figure 9a, e respectively shows the CF and IL responses of the outer pipe in the range of $0 \leq U_r \leq 50$ for $u=0$. As can be seen from Fig. 9a, the CF motion

amplitudes of the outer pipe are extremely small for relatively low U_r . When U_r is close to 4, the CF motion amplitudes increase sharply because the PIP system has generated a 'lock-in' phenomenon in the first mode of the inner pipe. The lock-in phenomenon of VIVs in the first mode occurs in the range of $4 \leq U_r \leq 7$ approximately. When U_r is higher than 7, the CF motion amplitudes decrease to relatively low values. In the range of $25 < U_r < 40$ approximately, the VIV responses of the outer pipe become strong, and they are mainly dominated by the second-mode component of a cantilevered beam. The IL responses of the outer pipe for $u=0$ are plotted in Fig. 9e, and the response amplitudes are shown to increase gradually to larger values when U_r is increased in the range of $0 \leq U_r \leq 50$.

Figure 9b, f respectively shows the CF and IL responses of the outer pipe in the range of $0 \leq U_r \leq 50$ for $u=5.0$. In this case, the axial flow velocity of the inner pipe is still below the lowest critical value for flutter instability of the PIP system. Figure 9b shows a bifurcation diagram different from that of Fig. 9a. It is seen that the first maximum amplitude of the VIV responses occurs at a higher value of U_r . Obviously, such a maximum amplitude is lower than

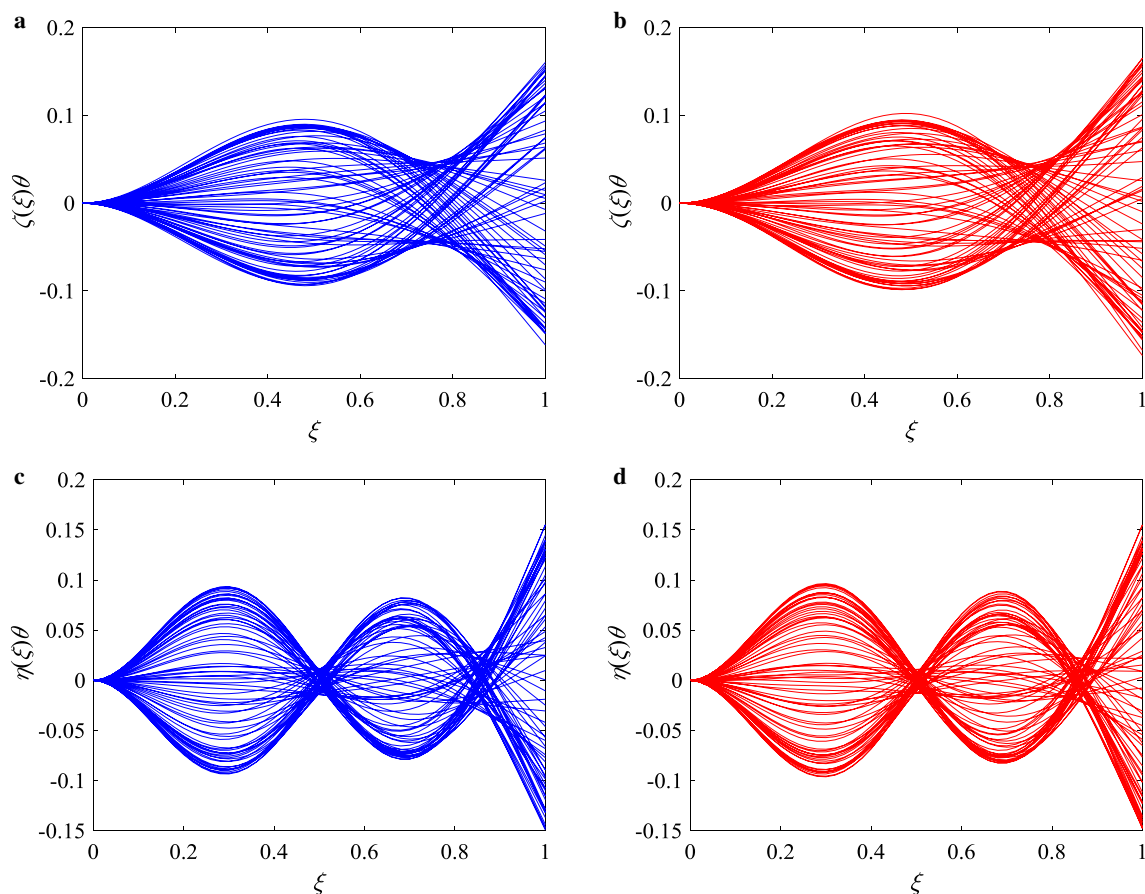


Fig. 7 Oscillation shapes of the PIP system for $U_r=44$ and $u=5$, **a, b** cross-flow motions of outer and inner pipes, respectively; **c, d** in-line motions with removal of the mean values of the outer and inner pipes, respectively

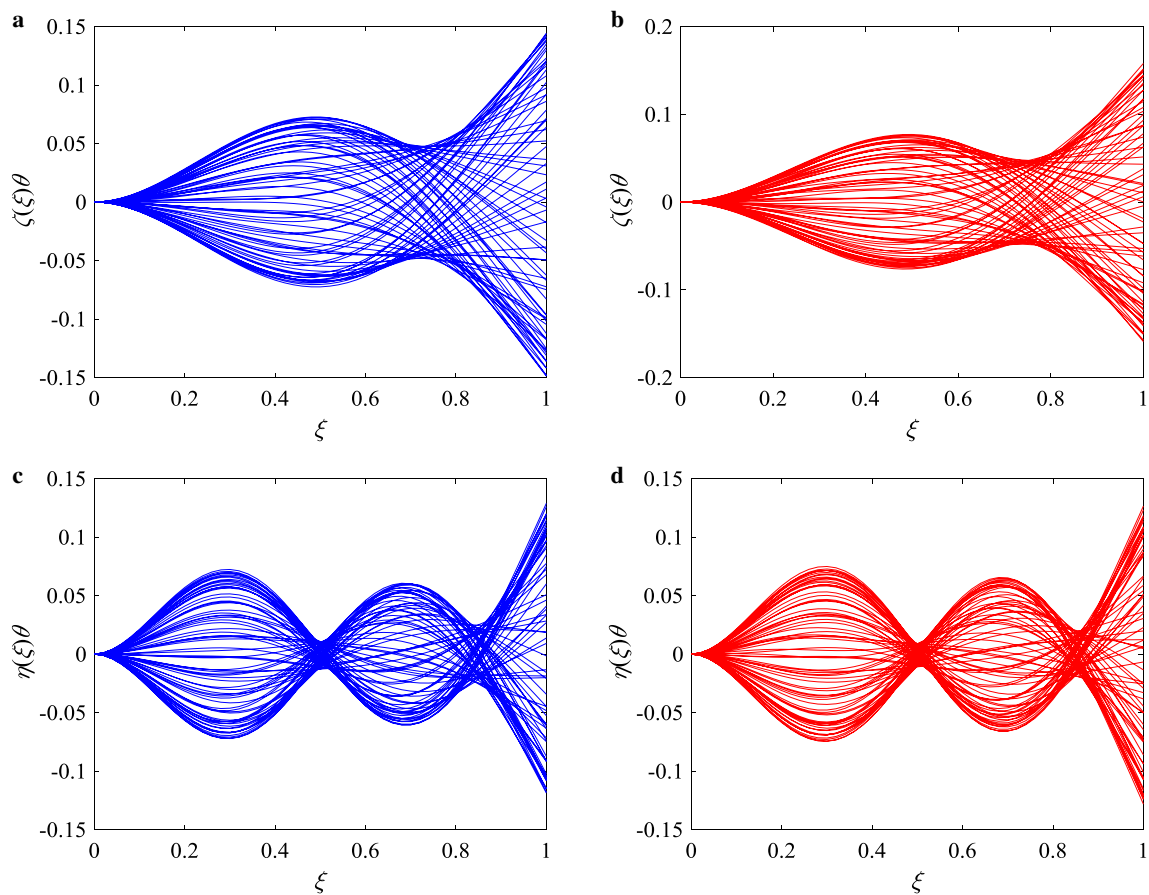


Fig. 8 Oscillation shapes of the PIP system for $U_r=44$ and $u=8$, **a, b** cross-flow motions of outer and inner pipes, respectively; **c, d** in-line motions with removal of the mean values of the outer and inner pipes, respectively

the counterpart shown in Fig. 9a. Indeed, the first mode of the inner pipe has a relatively large positive damping when $u = 5$ (see Fig. 3), thus yielding a lower amplitude of VIV response of the PIP system. The bifurcation diagram of Fig. 9f for $u = 5.0$ is qualitatively similar as that of Fig. 9e. For each value of U_r , however, the maximum amplitude of Fig. 9f is generally lower than that of Fig. 9e.

The next case we considered is a PIP system with the internal flow velocity equal to 6.6. In this case, the internal flow velocity is beyond the lowest critical value for internal flow-induced flutter instability of the outer pipe, while it is below the secondary critical value for flutter instability of the inner pipe. As shown in Fig. 9c, g, the most interesting dynamical feature of the PIP system with $u = 6.6$ is that either CF or IL response of the outer pipe has a perturbed displacement around the mean displacement position, even for sufficiently small cross-flow velocities. This new feature is due to the internal flow-induced flutter and is obviously different from that shown in Fig. 9b, f. Furthermore, the IL response amplitude shown in Fig. 9g for each U_r is obviously lower than that shown in Fig. 9f. This means that the

internal flow-induced flutter instability can reduce the IL responses of the PIP to some extent.

Now we turn our attention to the case of $u = 8$. The internal flow velocity in this case is higher than the two critical values for flutter instability. It is immediately seen from Fig. 9d that the overall dynamical behavior of the pipe for $u = 8$ is qualitatively similar to that of the pipe for $u = 6.6$. However, the initial perturbed displacements of the pipe for $u = 8$ are larger than that of the pipe for $u = 6.6$ due to the concurrent flutter instability of the inner and outer pipes. It is seen from Fig. 9h that the overall dynamical behavior of the IL responses for $u = 8$ is qualitatively similar to that shown in Fig. 9g. Therefore, in the range of $0 \leq U_r \leq 50$, it is found that the IL oscillation amplitudes of the outer pipe would decrease gradually with the increment of internal flow velocity. This trend can be clearly seen in Fig. 9e–h. To explore the rich dynamics of the PIP system, some typical results of phase portraits and trajectory diagrams of the outer pipe are further plotted in Figs. 10, 11, 12, 13.

The results shown in Fig. 10a–c are for $U_r = 30$ and $u = 0$, demonstrating that the dynamic response of the

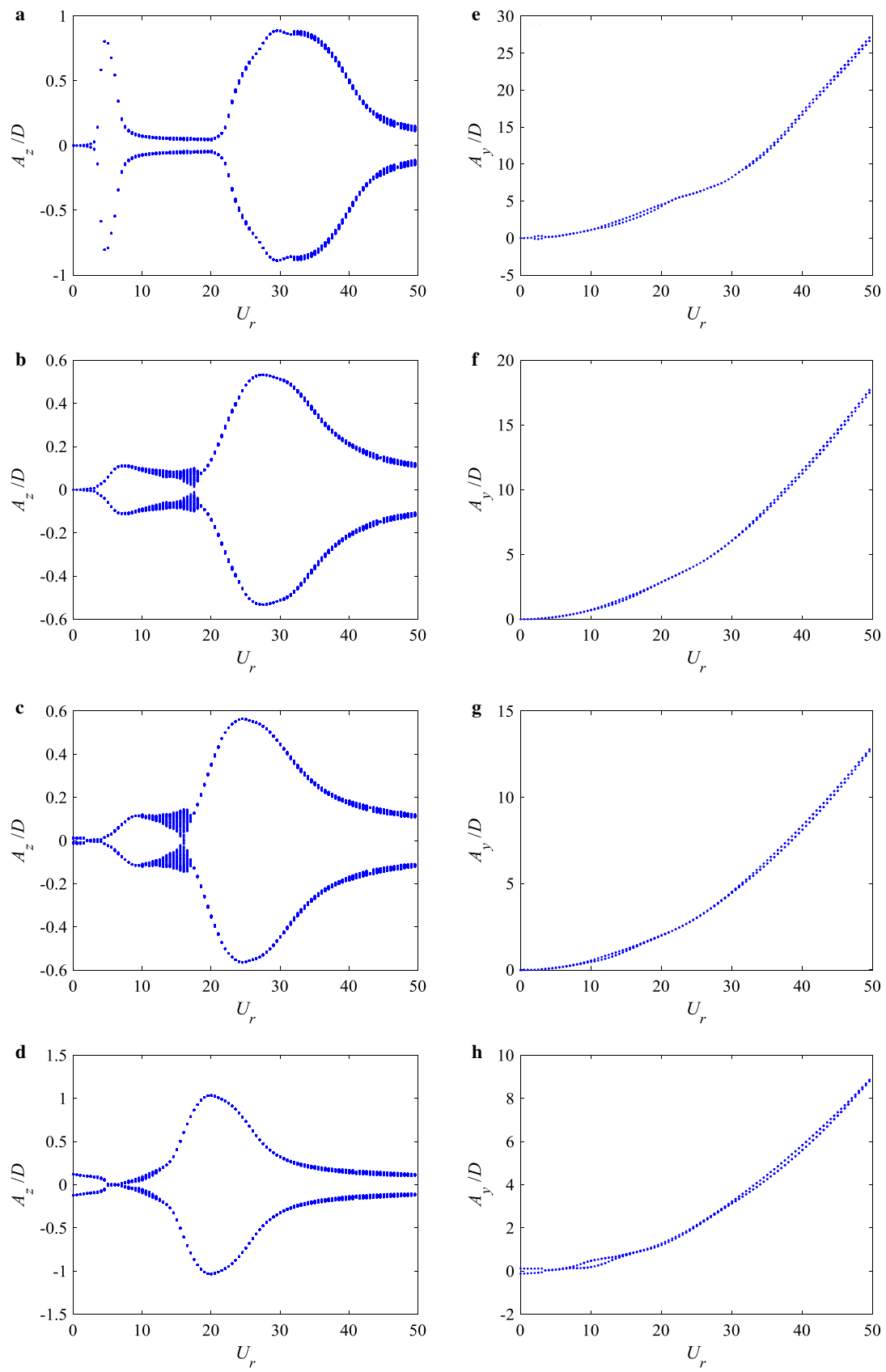


Fig. 9 Bifurcation diagrams of the outer pipe, with the reduced cross-flow velocity as the variable parameter: **a, e** cross-flow and in-line dimensionless tip displacements for $u=0$, respectively; **b, f** cross-flow and in-line dimensionless tip displacements for $u=5$, respectively; **c, g** cross-flow and in-line dimensionless tip displacements for $u=6.6$, respectively; and **d, h** cross-flow and in-line dimensionless tip displacements for $u=8$, respectively

outer pipe corresponds to a periodic motion. Figure 10a, b shows that the CF response of the outer pipe undergoes a limit-cycle motion, while it shows that the IL response of the outer pipe undergoes a multi-periodic motion. Figure 11 corresponds to the dynamic response of the outer pipe for $U_r=30$ with a subcritical internal flow velocity $u=5$, demonstrating that the PIP system undergoes

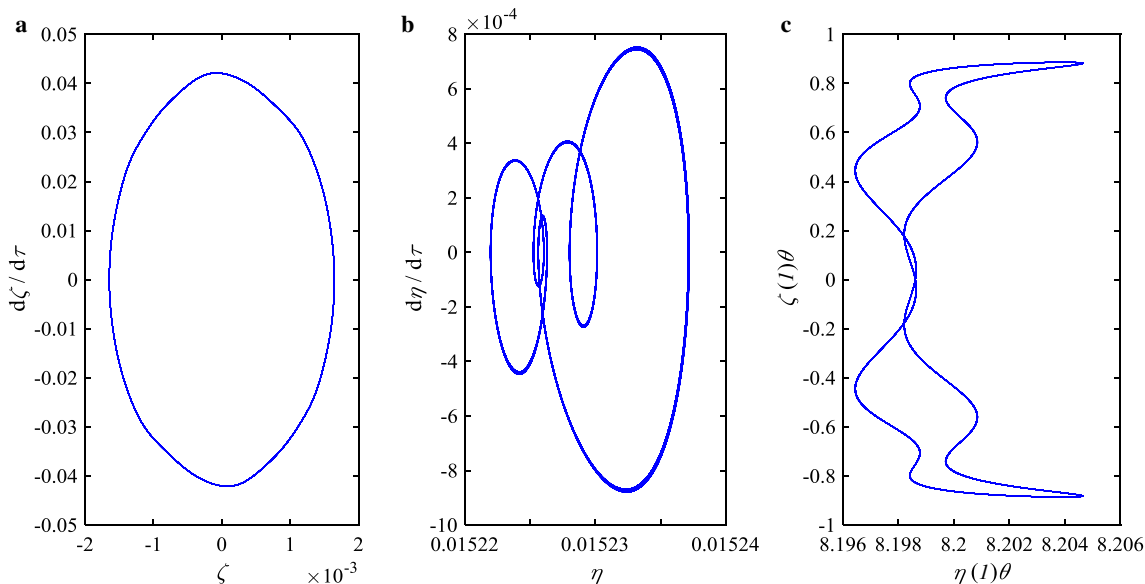


Fig. 10 Dynamic responses of the outer pipe at $\xi=1$ for $U_r=30$ and $u=0$, **a** phase portrait of CF motions, **b** phase portrait of IL motions, **c** oscillation trajectory

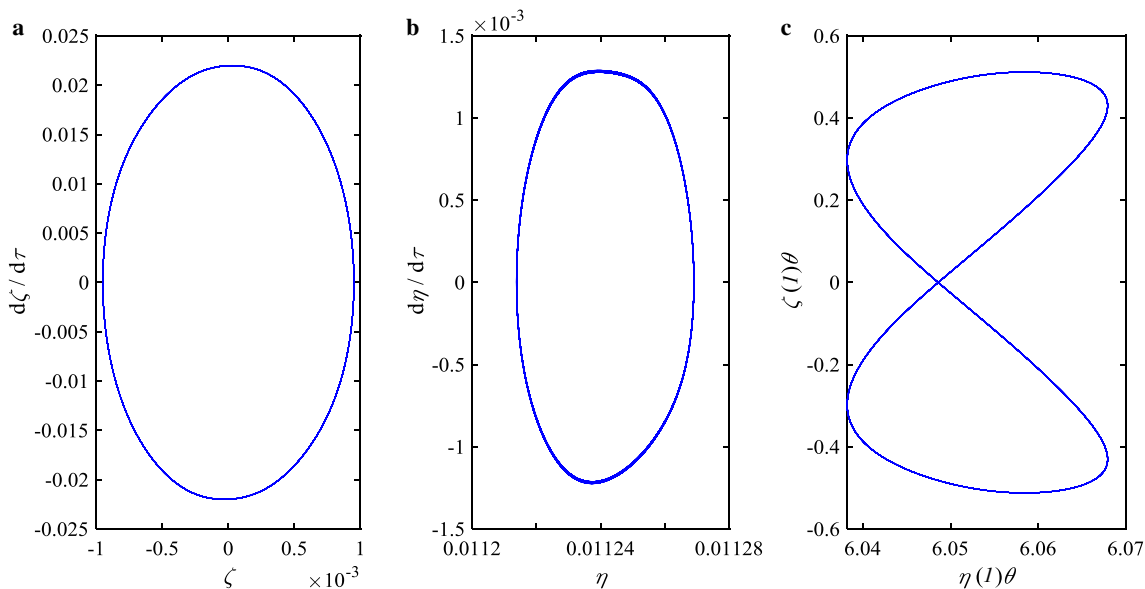


Fig. 11 Dynamic responses of the outer pipe at $\xi=1$ for $U_r=30$ and $u=5$, **a** phase portrait of CF motions, **b** phase portrait of IL motions, **c** oscillation trajectory

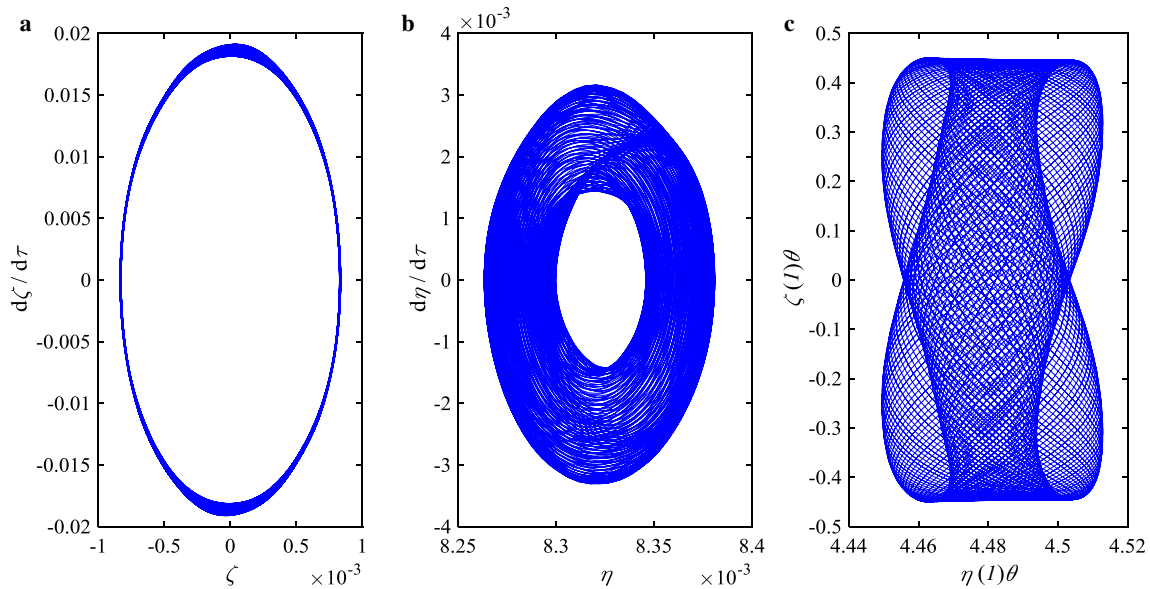


Fig. 12 Dynamic responses of the outer pipe at $\xi=1$ for $U_r=30$ and $u=6.6$, **a** phase portrait of CF motions, **b** phase portrait of IL motions, **c** oscillation trajectory

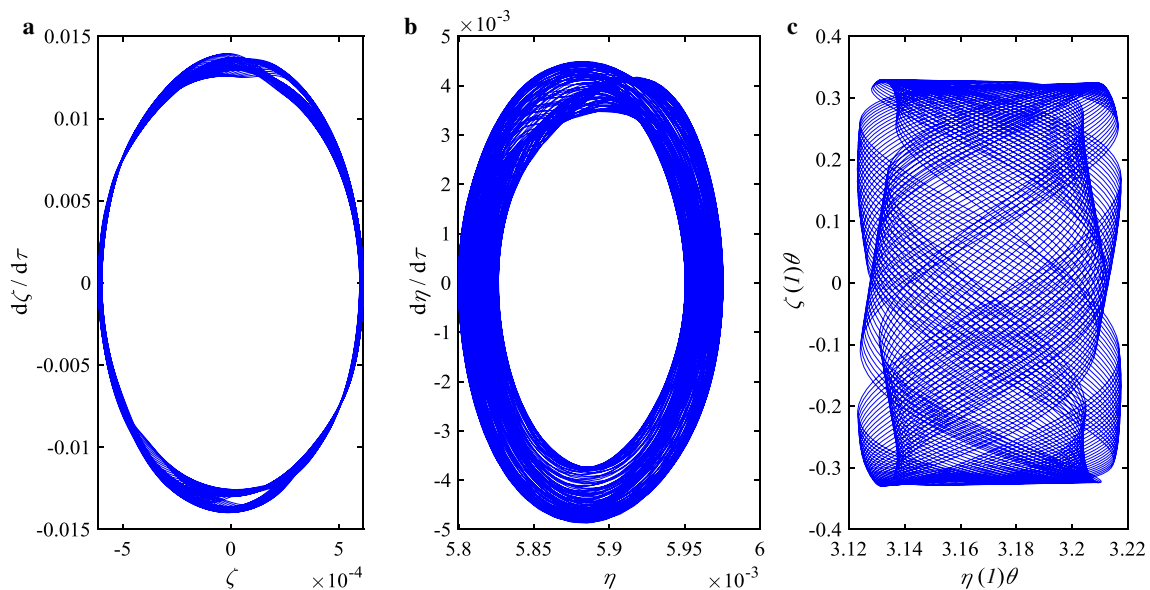


Fig. 13 Dynamic responses of the outer pipe at $\xi=1$ for $U_r=30$ and $u=8$, **a** phase portrait of CF motions, **b** phase portrait of IL motions, **c** oscillation trajectory

a periodic motion with the feature of a figure-of-eight trajectory.

For the supercritical internal flow velocity case, Figs. 12 and 13 respectively show the dynamic responses of the outer pipe for $u=6.6$ and $u=8$, with $U_r=30$. It is found that the PIP system undergoes a non-periodic motion for the two supercritical internal flow velocities as shown in Figs. 12 and 13.

4 Conclusion

In order to investigate the basic mechanism of FIVs of a cantilevered PIP system concurrently subjected to axial and cross flows, a new 3D theoretical prediction model is proposed. The inner and outer pipes are connected by an insulation layer. The effects of the insulation layer on the inner and outer pipes are modelled by a linear distributed

damper, a linear distributed spring and a nonlinear distributed spring. The wake dynamics of the external cross flow is modelled by two distributed van der Pol wake oscillators. The full 3D nonlinear partial differential equations for the two pipes and the wake are coupled. These governing equations are discretized first by Galerkin's method, resulting in a set of ordinary differential equations. Then, the obtained ordinary differential equations are further solved by using a fourth-order Runge–Kutta integration algorithm. According to the results presented in the form of an Argand diagram, oscillation shape diagrams, phase portraits and bifurcation diagrams, some conclusions can be drawn as follows.

(1) The Argand diagram for the cantilevered PIP structure system without cross flow is greatly different from that of a single cantilevered pipe. The first-mode flutter instability of the outer pipe can occur at an internal flow velocity lower than the counterpart of the inner pipe.

(2) The bifurcation diagrams of the PIP structure system without cross flow are also different from that of a single cantilevered pipe conveying fluid. When the internal flow velocity is beyond the lowest critical value for flutter instability of the outer pipe but is below the secondary critical value for flutter instability of the inner pipe, the displacement amplitudes at the free end of the PIP system increase slowly with increasing internal flow velocity. When the internal flow velocity is beyond the two critical values for flutter instability of both inner and outer pipes, interestingly, the displacement amplitudes at the free end of the PIP system increase exponentially.

(3) When the internal flow velocity is below the lowest critical value for flutter instability, the response of the PIP system is mainly due to cross-flow-induced vibrations. When the internal flow velocity is beyond the lowest critical flow velocity for flutter instability, the response of the pipe is mainly attributed to the internal flow for relatively low cross-flow velocities, while it is mainly attributed to both internal and cross flows for high cross-flow velocities.

(4) The PIP system may exhibit both periodic and non-periodic motions for the varied velocity of the internal or cross flow. The CF and IL responses of the PIP system are generally coupled. Therefore, both CF and IL displacements need to be taken into account in the FIV analysis of PIP systems.

In summary, this paper has two main contributions. First, a novel theoretical model for exploring the FIVs of PIP structures in the presence of both internal axial flow and external cross flow has been developed. This theoretical model is capable of predicting the nonlinear responses of the coupled PIP system. Currently, there exist several theoretical models for FIV analysis of a single pipe with both internal and external fluid flows; however, there is a lack of theoretical models for FIV analysis of the PIP

system concurrently subjected to both internal and external fluid flows. The second contribution of this work is that we have suggested a conception of suppressing FIVs of marine pipes. Recalling that the IL displacement of a single pipe conveying fluid can become very large (is of the same order of magnitude as $0.5 \times L$) due to axial- and/or cross-flow-induced vibrations [28, 34], it may be an effective way to suppress the nonlinear responses of marine pipes conveying fluid with optimal design of desired PIP structures.

Acknowledgements The work was supported by the National Natural Science Foundation of China (Grant 11622216).

References

1. Yettou, E., Derradji-Aouat, A., Williams, C.: Fluid-Structure Interactions Modelling of PIP Riser Systems Operating in Ocean Environments. National Research Council Canada, Institute for Ocean Technology, St. John's (2008)
2. Sun, J., Jukes P.: From installation to operation: a full-scale finite element modeling of deep-water PIP system. In: Third ISOPE International Deep-Ocean Technology Symposium. International Society of Offshore and Polar Engineers, Beijing, May 31–June 5 (2009)
3. Sun, J., Jukes, P., Eltaher, A.: Exploring the challenges of pipe-in-pipe (PIP) flowline installation in deepwater. In: Third ISOPE International Deep-Ocean Technology Symposium. International Society of Offshore and Polar Engineers, Beijing, June 28–July 1 (2009)
4. Wang, Z., Chen, Z., Liu, H.: Numerical study on upheaval buckling of pipe-in-pipe systems with full contact imperfections. *Eng. Struct.* **99**, 264–271 (2015)
5. Karampour, H., Alrsai, M., Albermani, F., Guan, H., Jeng, D.S.: Propagation buckling in subsea pipe-in-pipe systems. *J. Eng. Mech.* **143**, 04017113 (2017)
6. Kyriakides, S.: Buckle propagation in pipe-in-pipe systems: part I. Experiments. *Int. J. Solids Struct.* **39**, 351–366 (2002)
7. Kyriakides, S., Vogler, T.J.: Buckle propagation in pipe-in-pipe systems: part II. Analysis. *Int. J. Solids Struct.* **39**, 367–392 (2002)
8. Kyriakides, S., Netto, T.A.: On the dynamic propagation and arrest of buckles in pipe-in-pipe systems. *Int. J. Solids Struct.* **41**, 5463–5482 (2004)
9. Gong, S.F., Li, G.: Buckle propagation of pipe-in-pipe systems under external pressure. *Eng. Struct.* **84**, 207–222 (2015)
10. Skop, R.A., Balasubramanian, S.: A new twist on an old model for vortex-excited vibrations. *J. Fluids Struct.* **11**, 395–412 (1997)
11. Evangelinos, C., Karniadakis, G.E.: Dynamics and flow structures in the turbulent wake of rigid and flexible cylinders subject to vortex-induced vibrations. *J. Fluid Mech.* **400**, 91–124 (1999)
12. Balasubramanian, S., Haan, F.L., Szweczyk, A.A., et al.: An experimental investigation of the vortex-excited vibrations of pivoted tapered circular cylinders in uniform and shear flow. *J. Wind Eng. Ind. Aerodyn.* **89**, 757–784 (2001)
13. Lin, L.M., Ling, G.C., Wu, Y.X., et al.: Nonlinear fluid damping in structure-wake oscillators in modeling vortex-induced vibrations. *J. Hydrodyn. Ser. B* **21**, 1–11 (2009)

14. Srinil, N.: Analysis and prediction of vortex-induced vibrations of variable-tension vertical risers in linearly sheared currents. *Appl. Ocean Res.* **33**, 41–53 (2011)
15. Dai, H.L., Wang, L., Qian, Q., et al.: Vortex-induced vibrations of pipes conveying pulsating fluid. *Ocean Eng.* **77**, 12–22 (2014)
16. Gu, J.J., Duan, M.L.: Integral transform solution for fluid force investigation of a flexible circular cylinder subject to vortex-induced vibrations. *J. Mar. Sci. Technol.* **21**, 663–678 (2016)
17. Wang, L., Jiang, T.L., Dai, H.L.: Three-dimensional dynamics of supported pipes conveying fluid. *Acta. Mech. Sin.* **33**, 1065–1074 (2017)
18. Nishi, Y., Motoyoshi, M., Ueda, T.: Growth and coexistence of structural and lift force modes in vortex-induced vibration of a flexible riser. *J. Mar. Sci. Technol.* **23**, 899–914 (2018)
19. Bi, K., Hao, H.: Using PIP systems for subsea pipeline vibration control. *Eng. Struct.* **109**, 75–84 (2016)
20. Zarei, M.S., Kolahchi, R., Hajmohammad, M.H., et al.: Seismic response of underwater fluid-conveying concrete pipes reinforced with SiO₂ nanoparticles and fiber reinforced polymer (FRP) layer. *Soil Dyn. Earthq. Eng.* **103**, 76–85 (2017)
21. Hajmohammad, M.H., Kolahchi, R., Zarei, M.S., et al.: Earthquake induced dynamic deflection of submerged viscoelastic cylindrical shell reinforced by agglomerated CNTs considering thermal and moisture effects. *Compos. Struct.* **187**, 498–508 (2018)
22. Hajmohammad, M.H., Maleki, M., Kolahchi, R.: Seismic response of underwater concrete pipes conveying fluid covered with nano-fiber reinforced polymer layer. *Soil Dyn. Earthq. Eng.* **110**, 18–27 (2018)
23. Matin, Nikoo H., Bi, K., Hao, H.: Passive vibration control of cylindrical offshore components using PIP (PIP) concept: an analytical study. *Ocean Eng.* **142**, 39–50 (2017)
24. Matin, Nikoo H., Bi, K., Hao, H.: Effectiveness of using PIP (PIP) concept to reduce vortex-induced vibrations (VIV): three-dimensional two-way FSI analysis. *Ocean Eng.* **148**, 263–276 (2018)
25. Yang, Z.M., Thorkildsen, F., Norland, K.: Vortex induced vibrations and fatigue assessment of pipe-in-pipe systems. In: *Proceedings of the ASME 2018 37th International Conference on Ocean, Offshore and Arctic Engineering*. American Society of Mechanical Engineers, Madrid, 17–22 June (2018)
26. Williams, D., Kenny, F.: Calculation of VIV fatigue of multi-pipe systems. In: *ASME 2017 36th International Conference on Ocean, Offshore and Arctic Engineering*. American Society of Mechanical Engineers, Trondheim, 25–30 June (2017)
27. Wadham-Gagnon, M., Paidoussis, M.P., Semler, C.: Dynamics of cantilevered pipes conveying fluid. Part I: nonlinear equations of three-dimensional motion. *Journal of Fluids and Structures* **23**, 545–567 (2007)
28. Liu, Z.Y., Wang, L., Dai, H.L., et al.: Nonplanar vortex-induced vibrations of cantilevered pipes conveying fluid subjected to loose constraints. *Ocean Eng.* **178**, 1–19 (2019)
29. Wang, L., Jiang, T.L., Dai, H.L., et al.: Three-dimensional vortex-induced vibrations of supported pipes conveying fluid based on wake oscillator models. *J. Sound Vib.* **422**, 590–612 (2018)
30. Facchinetti, M.L., de Langre, E., Biolley, F.: Coupling of structure and wake oscillators in vortex-induced vibrations. *J. Fluids Struct.* **19**, 123–140 (2004)
31. Ge, F., Long, X., Wang, L., et al.: Flow-induced vibrations of long circular cylinders modeled by coupled nonlinear oscillators. *Sci. China Ser. G Phys. Mech. Astron.* **52**, 1086–1093 (2009)
32. Munir, A., Zhao, M., Wu, H., et al.: Numerical investigation of the effect of plane boundary on two-degree-of-freedom of vortex-induced vibration of a circular cylinder in oscillatory flow. *Ocean Eng.* **148**, 17–32 (2018)
33. Yang, W.W., Ai, Z.J., Zhang, X.D., et al.: Nonlinear three-dimensional dynamics of a marine viscoelastic riser subjected to uniform flow. *Ocean Eng.* **149**, 38–52 (2018)
34. Paidoussis, M.P., Li, G.X., Moon, F.C.: Chaotic oscillations of the autonomous system of a constrained pipe conveying fluid. *J. Sound Vib.* **135**, 1–19 (1989)
35. Xu, J., Huang, Y.Y.: Bifurcations of a cantilevered pipe conveying steady fluid with a terminal nozzle. *Acta. Mech. Sin.* **16**, 264–272 (2000)
36. Ghayesh, M.H., Paidoussis, M.P.: Three-dimensional dynamics of a cantilevered pipe conveying fluid, additionally supported by an intermediate spring array. *Int. J. Non-Linear Mech.* **45**, 507–524 (2010)
37. Dai, H.L., Abdelkefi, A., Wang, L.: Theoretical modeling and nonlinear analysis of piezoelectric energy harvesting from vortex-induced vibrations. *J. Intell. Mater. Syst. Struct.* **25**, 1861–1874 (2014)
38. Wang, L., Liu, Z.Y., Abdelkefi, A., et al.: Nonlinear dynamics of cantilevered pipes conveying fluid: towards a further understanding of the effect of loose constraints. *Int. J. Non-Linear Mech.* **95**, 19–29 (2017)
39. Dai, H.L., Wang, L., Qian, Q.: Vortex-induced vibrations of pipes conveying fluid in the subcritical and supercritical regimes. *J. Fluids Struct.* **39**, 322–334 (2013)
40. Song, L.J., Fu, S.X., Cao, J., et al.: An investigation into the hydrodynamics of a flexible riser undergoing vortex-induced vibration. *J. Fluids Struct.* **63**, 325–350 (2016)
41. Bokaian, A.: Thermal expansion of PIP systems. *Mar. Struct.* **17**, 475–500 (2004)
42. Wang, F.C.: Effective design of submarine PIP using finite element analysis. *Ocean Eng.* **153**, 23–32 (2018)